# Effects of Ta doping and irradiation with He+ ions on photoluminescence of MgAl2O4 spinel ceramics

H. Spiridigliozzi, A. Pille, F. Schoenstein, L. Museur, E. Feldbach, H. Mändar, M. Kitaura, Andrei Kanaev

# Effects of Ta doping and irradiation with $He^+$ ions on photoluminescence of $MgAl_2O_4$ spinel ceramics

H. Spiridigliozzi [a], A. Pille [a], F. Schoenstein [a], L. Museur [b], E. Feldbach [c], H. Mändar [c], M. Kitaura [d], A. Kanaev [a *]

[a] *Laboratoire des Sciences des Procédés et des Matériaux, CNRS, Université Paris 13, 93430 Villetaneuse, France*
[b] *Laboratoire de Physique des Lasers, CNRS, Université Paris 13, 93430 Villetaneuse, France*
[c] *Institute of Physics, University of Tartu, 1 W. Ostwald str., 50411, Tartu, Estonia*
[d] *Faculty of Science, Yamagata University, 1-4-12 Kojirakawa, Yamagata 990-8560, Japan*

Received XX Month XXXX; accepted XX Month XXXX

**Abstract**

Photoluminescence (PL) properties of pristine and Ta-doped $MgAl_2O_4$ spinel ceramics prepared via spark plasma sintering technique and irradiated with $He^+$ ions were studied. The results indicate strong influence of the grain boundaries on PL spectra. Ta doping promotes the formation of O and Al vacancies at the grain boundaries leading to an increased number density of $F^+$ centres. The ionised irradiation forms antisites preferentially at the grain boundaries, which inhibit excitonic PL and exciton energy transfer while do not affect proper PL of lattice defects. A weak PL excitation band at 7.25±0.25 eV may belong to excitons localised near bulk antisites. In the Ta-doped ceramics, the electronic transitions between 5.75 eV and 7.0 eV belong to an intermediate state situated at the grain boundaries and structurally linked to Ta, which readily transfers energy to F and $F^+$ centres; it was assigned to the nucleated $Mg_4Ta_2O_9$ phase.

*Keywords: $MgAl_2O_4$ ceramics, $Ta_2O_5$ doping, Spark plasma sintering, Photoluminescence, $He^+$ irradiation*

## 1. Introduction

Compounds with the spinel structure have been predicted to exhibit a very high tolerance to irradiation with fast neutrons resulting in low swelling even at high doses [1]. In this connection, the understanding of their electronic band structure and defects induced by ionized radiation is of paramount importance for the development of novel optical materials stable in the environments of a fusion reactor. Between them, $MgAl_2O_4$ spinel is a well known material of a strong practical interest, which electronic and optical properties in connection with radiation-induced damage require more understanding, especially of its ceramic form.

One important aspect of the practical interest is connected with nanocrystalline ceramics, which have been shown to possess an improved radiation tolerance. This improvement is due to large fraction of grain boundaries, which act as sinks of elementary radiation defects (vacancy and interstitials) where healing of crystal structure occurs via recombination and annihilation of these primary defects (see [2-4] and references therein). The main practical difficulty of producing nanocrystalline ceramics is that the crystalline domains tend to grow during the sintering stage. This is why the designing materials with interfaces appropriate for defects annihilation has seen a limited success in technological applications and relevant publications on the successful nanoceramics realization are very rare [5, 6]. One possibility to prevent the grain growth is the addition of an inhibitor [7].

In this study, we performed spectroscopic analysis of $MgAl_2O_4$ spinel ceramics, prepared with Spark Plasma Sintering (SPS) with $Ta_2O_5$ inhibitor, by means of energy-resolved photoluminescence (PL) spectroscopy, which is widely acknowledged as a powerful tool for evaluation of the electronic defect structure of optical materials. The use of PL excitation (PLE) in vacuum UV range was inevitable due to wide band-gap of $MgAl_2O_4$ spinel.

## 2. Experimental

The precursor powder of $MgAl_2O_4$ spinel from Sasol Germany with impurity content below 5 ppm was used without any pretreatment. The particles have a size distribution D50 with the mean grains size ~20 μm and crystallite size ~115 nm. $Ta_2O_5$ powder (ChemPur) with purity 99.9 % and averaged size of 500 nm was used as an inhibitor of the grain size growth during sintering. A small quantity of this powder between d=0.5 and 4 wt% was added to the spinel powder and grinded in an agate mortar until the homogeneous mixture was obtained.

The sintering was performed via spark plasma sintering (SPS) method using Dr. Sinter LAB Series SPS-515S device, employing maximum force of 50 kN, temperature 2000 °C and heating rate of 600 °C/min with a peak current of 1500 A. The sintering was conducted under primary

* Corresponding author. Tel: +33-1-49403430; fax: +33-1-49403414;
E-mail: andrei.kanaev@lspm.cnrs.fr

vacuum of 10 Pa. During the preparation, about 1.5 g of powder was load in a graphite mold of 1.5 cm internal diameter. In our previous study of the spinel ceramics sintering from the commercial powders (Sasol) [8], the preference of the short dwell has been confirmed in preventing the grain growth and attaining the finest microstructure. Consequently, 3 min dwell time of the dilatometric sintering cycle was applied in the present study, as Fig. 1 shows. After a plateau of 600 °C for 10 min, served to purify the powder from traces of the adsorbed water, the temperature was incremented by 50 °C/min up to the maximum of 1650 °C. The maximum pressure of 80 MPa was maintained during the increment and maximum temperature application.

The recovered ceramic pellets after SPS sintering (with a hardness 8-8.5 on the Mohs scale) were mirror-polished to 1.0 mm thickness with diamond pastes containing abrasive particles of 0.25 μm size. The pellets were heat treated at a reduced temperature 1300 °C with respect to the sintering one for 1 hour under ambient air in order to relax internal mechanical constraints and fill oxygen vacancies that may appear during SPS processing.

The mass density of the pellets was measured by helium pycnometer (micromeritics AccuPyc II 1340). The relative density was calculated assuming the bulk mass density $\rho_0$=3.578 g/cm$^3$ of $MgAl_2O_4$ spinel [9]. The transmittance test of the prepared ceramics was realised in the near-IR-visible-UV spectral range using Lambda 35 UV/Vis spectrometer (PerkinElmer, France) at the normal incidence of the collimated light beam, with the detector placed at 1 cm behind a pellet (solid angle of the reception ~1 rad).

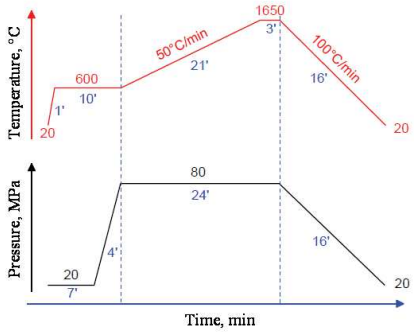


Fig. 1. Sintering cycle applied to $MgAl_2O_4$ ceramics preparation. Times of P-T application are indicated below cycle lines.

The surface morphology including sizes of crystalline domains was characterized using Scanning Electron Microscopy (SEM) installation ZEISS GEMINI SUPRA 40VP FEG. The spatial maps of O, Al, Mg and Ta elements were measured after EDX analysis using SEM (LEO PGT LEICA S440, W filament) installation. Preliminary to these measurements, the dielectric pellets were covered with carbon (Gatan Model 682, PECS). XRD analysis was performed on diffractometer *SmartLab* (Rigaku) using Cu rotating anode working at 45kV and 180mA, coordinate sensitive 1D detector D/teX Ultra and Bragg-Brentano optical setup. Diffraction patterns were measured with step 0.01° (2θ) and step scan time 0.08 sec. The calibration has been performed with SRM 640 reference. Program *TOPAS 6 Academic* was used for the cell parameter and sample displacement refinement. Absolute errors of parameters were calculated at confidence level of 99% from standard deviations by using Student test method (by using multiplier of 2.86 at standard deviations).

The photoluminescence (PL) experiments were carried out at the BL3B beamline [10] of UVSOR facility with synchrotron radiation (SR) excitation in the UV-visible spectral range. The samples were mounted on the cold finger of a LHe flow type cryostat, which permitted stabilizing the sample temperature in the range between 300 and 8 K. The vacuum in the samples chamber was ~$3\cdot10^{-7}$ Pa. In order to evaluate structural damage induced by the ionized irradiation, PL and PL excitation (PLE) spectra of as-prepared and irradiated ceramics were compared. The measured PLE spectra were corrected on the detector sensitivity and optical line transmission. The irradiation of the spinels with 150 keV energy $He^+$ ions of the total dose $10^{17}$ cm$^{-2}$ was performed in the Accelerator Lab of Helsinki University.

## 3. Results and discussion

The pellets transparency in the visible spectral range at 550 nm decreased with an increase of the Ta content. The pellets were partially transparent for relatively low doping with $Ta_2O_5$ with the transmittance 30 % (d=0) and 7 % (d=1 wt%), while they become opaque for stronger doping d≥2 wt%. A more complex analysis of the transmittance, separating absorbance and scattering contributions, was not realized in this study. However, the decrease of transparency in the visible spectral range (visible by a naked eye) was clearly attributed to the light scattering due to pellets porosity appearing with the $Ta_2O_5$ addition.

The mass densities of the obtained ceramics listed in Table 1 were close to $\rho_0$ of the bulk solid with the relative density of <99%, indicating a low residual porosity after the sintering stage. In the same time, these results show that a small insertion of $Ta_2O_5$ (d=0.5 wt%) decreases the mass density of the obtained spinel ceramics. Our results indicate that this is related to a small residual porosity after the sintering, induced by the dopant. At higher doping level d≥1 wt%, the increase of the bulk mass density can be related to the new $Mg_4Ta_2O_9$ phase formation, which mass density 6.17 g.cm$^{-3}$ [11] is appreciably higher than that of spinel ($\rho_0$).

Table 1. Mass density of spinel ceramics with different $Ta_2O_5$ addition.

| d (wt%) | 0 | 0.5 | 1 | 2 | 4 |
|---|---|---|---|---|---|
| ρ (g.cm$^{-3}$) | 3.575(6) | 3.540(7) | 3.563(8) | 3.586(9) | 3.594(5) |
| $\rho/\rho_0$ (%) | 99.9(2) | 99.0(2) | 99.6(2) | 100.2(2) | 100.4(1) |

The X-ray diffraction patterns evidence pure spinel phase in ceramics with low Ta doping d≤1 wt% (Fig. 2). For doping with d≥1 wt% a new crystalline phase appeared, which was identified with the composition $Mg_4Ta_2O_9$ [12]. The relative volume of this phase increases with doping

from 0.4 % (d=2 wt%) to 2.0% (d=4 wt%). For a smaller Ta content the percentage of this phase could not be evidenced, probably because of its small mass, while inset in Fig. 2 clearly shows its presence at 1 wt% Ta. In the same time, pure $Ta_2O_5$ phase was not detected, which apparently signify its reaction with the host material during the sintering stage. An extremely weak periclase MgO contamination (peak at 41.3°) could be also noticed. The Rietveld refinement of X-ray diffractograms performed with TOPAS software showed no significant changes of the cell parameter with doping. We obtained $a$=8.0835(1) for d=0 and $a$=8.0867(1) Å for d=1 wt%. This indicated a weak insertion of Ta in the spinel structure, which is expectable due to a significant mismatch of the Van der Waals radii, equal to 0.3 Å between Ta and Al and 0.5 Å between Ta and Mg elements. The analysis based on the correlation between the lattice parameter and degree of inversion [13] evidenced the inversion or disorder parameter of the synthesized ceramics in the range of i≈0.15, which is defined as the fraction of octahedral sites occupied by $Mg^{2+}$ in $(Mg_{1-2i}Al_{2i})[Mg_{2i}Al_{2-2i}]O_4$. A non-negligible inversion i>0 could be expected in the spinels ceramics because of a low formation energy of antisites and high energy input during the sintering. However, the inversion parameter is close to that of the precursor powder with the lattice parameter $a$=8.0875 Å, showing the major role of the precursor material in the ceramics properties.

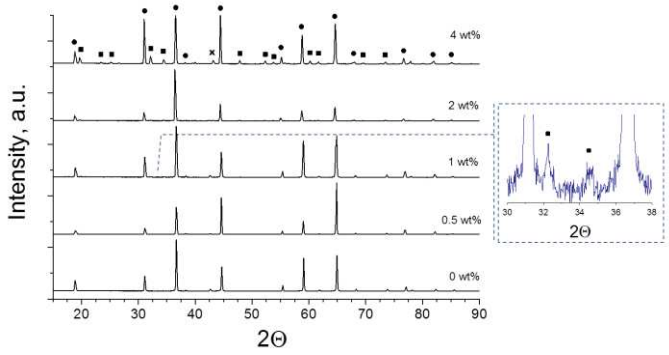


Fig. 2. X-ray diffraction patterns of $MgAl_2O_4$ ceramics (Ta doping is indicated). Peaks of $MgAl_2O_4$ (●), $Mg_4Ta_2O_9$ (■) and MgO (✖) phases are labelled. Inset shows $Mg_4Ta_2O_9$ peaks already at 1 wt% $Ta_2O_5$ doping.

The ceramics grains generally show a bimodal size distribution [8]. Two examples of SEM images of the prepared $MgAl_2O_4$ spinels ceramics with d=0.5 wt% and 1 wt% are shown in Fig. 3, characterized by rather large grains polydispersity with the mean size of about 5 μm and the first maximum at about 1 μm. The backscattering electron images indicate bright rims surrounded crystalline grains. The bright clusters, more numerous in 1wt% doped ceramics compared to 0.5 wt% doped one, indicate their connection with Ta. We tentatively attribute this core-rim morphology to the Ta rich phase concentrated at the $MgAl_2O_4$ spinel grains boundaries. Whether this phase belongs to $Ta_2O_5$ or $Mg_4Ta_2O_9$ remains an issue at least for a small doping d≤0.5 wt%. However, our further XRD analysis evidenced the appearance of $Mg_4Ta_2O_9$ crystallites at least for $Ta_2O_5$ doping of 1 wt% and higher. This new phase does not homogeneously cover the spinel crystallites but nucleates in the junction points between several grains, which apparently takes place at low doping ≤0.5 wt%, than expanding along the grain boundaries at larger doping ≥1 wt%. The halo visible in the rim regions may be due to Ta diffusion.

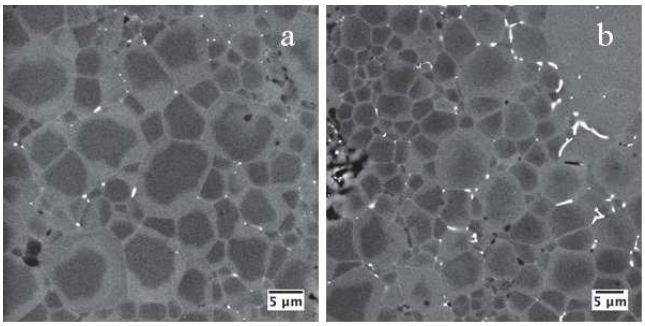


Fig. 3. SEM images of $MgAl_2O_4$ ceramics with 0.5 wt% (a) and 1 wt% $Ta_2O_5$.

The results of EDX measurements confirm a high homogeneity of the spinel composition by mapping O, Mg and Al elements in absence of Ta. In contrast, spatial distribution of Ta over the solid was not homogeneous, as Fig. 4 shows for 1 wt% $Ta_2O_5$ doping. In fact, white spots in the SEM image correspond to the electron backscattering from a heavy element as confirmed by Ta mapping. Ta tends to accumulate at the grain boundaries avoiding bulk dissolution. This is in agreement with the conclusion of X-ray diffraction measurements about a weak Ta insertion in the spinel structure. Moreover, zones of the Ta enrichment have a lack of Al and O elements but no significant variation of Mg content. In agreement with XRD patterns, this further leads to the nucleation of $Mg_4Ta_2O_9$ phase. We notice that the new phase may not be formed in all zones enriched by Ta but only in those with the critical enrichment, which remains beyond the scope of this study. The halo zones (Fig. 3) with the relatively low Ta concentration fail below EDX sensitivity limit and escape the analysis.

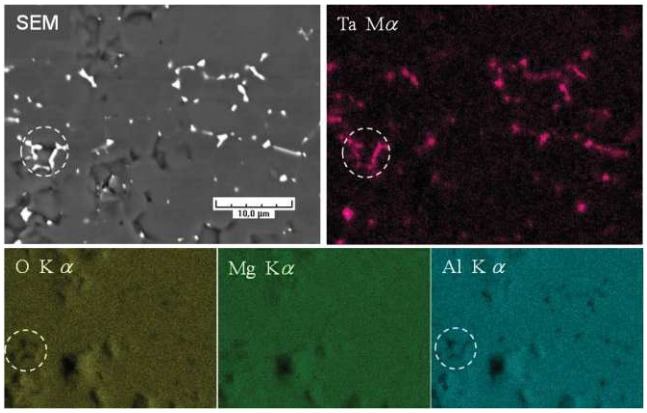


Fig. 4. SEM and EDX elemental maps of $MgAl_2O_4$ ceramics with 1 wt% $Ta_2O_5$. A representative zone of Ta enrichment and lack of O and Al elements is shown by dotted circle.

The PL spectra of pristine and Ta-doped $MgAl_2O_4$ spinels are shown in Fig. 5. They include five principal bands labeled UV1, UV2, V1, V2 and NIR, which have been previously discussed in literature. The UV1 band at 228 nm (5.44 eV) has been assigned to the recombination of conduction-band electrons with holes captured at the nearby oxygen ions [14]. The broad PL band situated between 2.5 and 4.5 eV can be decomposed in two well resolved sub-bands: V1 with the maximum at 410 nm (3.0 eV) and UV2 at 320 nm (3.9 eV), which can be respectively assigned to $F^+$ centres (one electron trapped at oxygen vacancy) [15] and F centres (two electrons trapped at oxygen vacancy) [8]. The V2 band at 520 nm (2.4 eV) belongs to tetrahedrally coordinated $Mn^{2+}$ impurity [14] and the most long-wavelength structured near-infrared (NIR) band at ~700 nm (1.8 eV) is due to well-known R-lines of $Cr^{3+}$ impurity [16].

The presence of Ta in the spinel structure affects intensities of these PL bands. While intensities of NIR and UV2 bands do not change with Ta doping, the intensity of V1 band significantly increases and that of V2 band decreases. Moreover, the intensities of UV1 and V2 bands strongly correlated and the addition of Ta suppressed them by the same factor of 10. Our EDX analysis in Fig. 4 showed a net correlation between spatial zones enriched with Ta and O and Al depletion. This apparently affects the population of $F^+$ centres formed of O vacancies, which can be promoted in the material by the removal of O and Al elements from the structure, resulting in the V1 band enhancement. Since band gap energy of solid $Ta_2O_5$ is 3.9 eV [17], the related interband absorption can appear at $\lambda \leq 320$ nm, which might explain the attenuation of UV1 PL. However, we reject this hypothesis, since PL excited at 157 nm comes from a thin layer of 1/k~100 nm thickness (k is characteristic absorption coefficient at direct transitions in semiconductors) while penetration depth of UV1 photons (228 nm) in 1 wt% "diluted" $Ta_2O_5$ solid is much longer ~10 μm. Consequently, the interband $Ta_2O_5$ absorption cannot explain strong UV1 band attenuation observed in the experiment. We conclude that a quenching phenomenon is responsible for this effect.

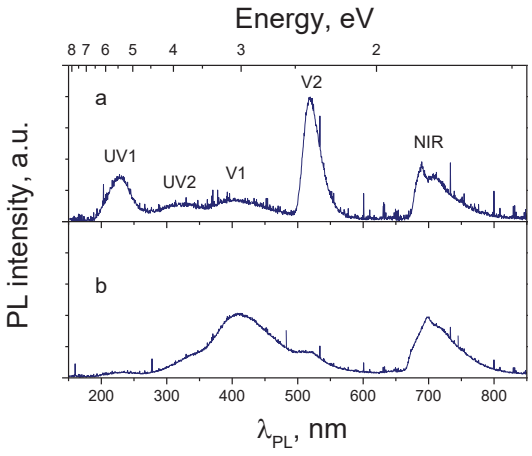


Fig. 5. PL spectra of non-irradiated $MgAl_2O_4$ ceramics without (a) and with 1 wt% $Ta_2O_5$ (b) addition (excitation at 157 nm, T=9 K).

The PLE spectra of pristine and Ta-doped $MgAl_2O_4$ spinels, respectively in Fig. 6 and Fig. 7, permit a deeper insight into the structural modifications. They are shown together with PLE spectra of the ceramics after irradiation with $He^+$ ions. The minimum of PLE spectrum at $E_g$=8.3±0.1 eV of the most short wavelength UV1 PL band in Fig. 6 can be attributed to the fundamental absorption onset and assigned to the band gap energy of $MgAl_2O_4$ spinel. This value is somewhat higher than those earlier obtained from optical reflection and transmission measurements 7.8 eV [18] and 8.0 eV [19] and theoretical predictions (see e.g. 7.5 eV in ref. [20]), which generally underestimate this energy. In the same time, it is close to that 8.2 eV recently suggested for spinel single crystals, based on the analysis of low temperature (6 K) PL/PLE spectra [21-22]. The interband electronic transitions $h\nu \geq 8.3$ eV can be also seen in PLE spectra of all emissions of pristine $MgAl_2O_4$ (Fig. 6), while they are less pronounced in UV1 PLE spectrum of Ta-doped ceramics (Fig. 7).

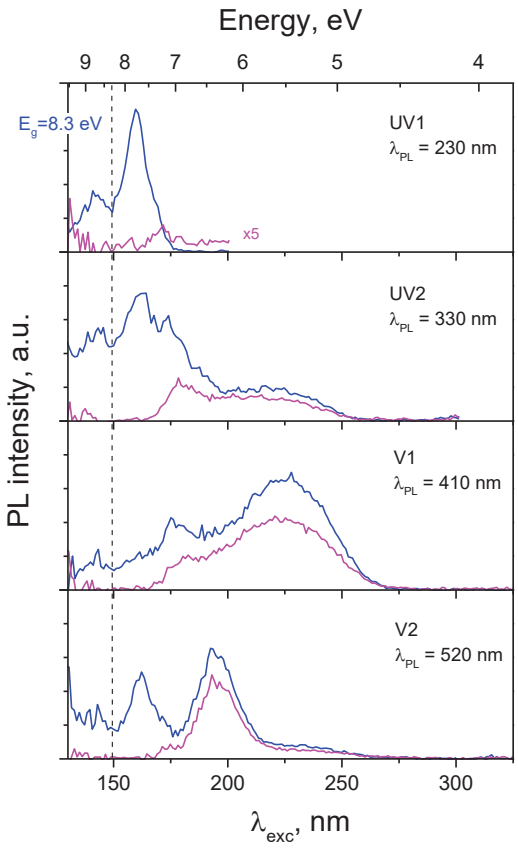


Fig. 6. PLE spectra of pure $MgAl_2O_4$ ceramics before (blue) and after (magenta) $He^+$ irradiation. PL bands and respective wavelengths are indicated (T=9 K).

The PLE band in the range of $7.0 \text{ eV} \leq h\nu \leq E_g$ with the maximum at 7.8 eV (Fig. 6) can be attributed to an exciton absorption and correspondent UV1 PL band at 5.44 eV in Fig. 5 to a localised exciton. The nature of the localisation sites still remains an issue, while very recent studies of the Tartu group [21-22] tentatively assigned them to antisite defects. The excitonic transitions at 7.8 eV were clearly

observed in PLE spectra of UV2 and V2 bands, which indicates an effective energy transfer from exciton to respectively F centres and $Mg^{2+}$ defects. In contrast, the energy transfer from excitons to $F^+$ centres (V1 band) was found ineffective since the respective PLE spectrum showed no signature of the excitonic transitions. This signifies rather complex energy transfer between the neutral (exciton) and charged ($F^+$) states. A strong correlation between UV1 and V2 PL supports an assumption about its substitutional position at tetrahedral sites of the spinel structure $Mn^{\times}_{Mg}$ (in Kröger-Vink notation). Below the band gap energy, PLE spectrum of V2 consists of almost one $Mg^{2+}$ band with the maximum at 6.35 eV (Fig. 6); a weak broad contribution from 7.35 eV to ~4.6 eV common with V1 can be explained by a superposition of the PL bands (Fig. 5).

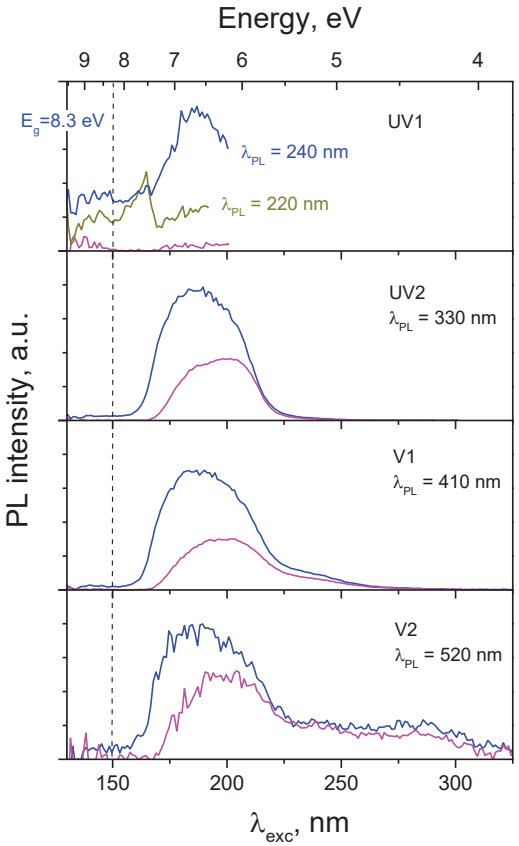


Fig. 7. PLE spectra of $MgAl_2O_4$ ceramics with 1 wt% $Ta_2O_5$ before (blue, gray) and after (magenta) $He^+$ irradiation. PL bands and respective wavelengths are indicated (T=9 K).

The irradiation of samples with $He^+$ ions weakened PL and strongly modified PLE spectra of all bands, except for that of $Cr^{3+}$ impurity (not shown). In particular, UV1 band was strongly suppressed, which is in agreement with previous observations of radioluminescence and cathodoluminescence of spinel crystals after irradiation with protons and neutrons [9, 16-18]. This effect, not specific to the nature of ionized particles, has been tentatively ascribed to a partial inversion of normal spinel and formation of antisite defects.

The most fundamental question from the point of view of radiation tolerance of spinel is how much antisites concentration can be increased after the irradiation. The damage profile in the irradiated layer of 0.5-0.6 μm thickness was simulated by SRIM software and indicated quite a high value of displacements per atom, up to 0.5 dpa at the maximum of distribution [24], which can be interpreted as a full amorphisation of the material. However, a significant part of this displacement is expected to recombine during the irradiation, which makes the real concentration of antisites smaller [25]. The detailed analysis of PL in $He^+$-irradiated samples is complicated because the penetration depth of photons does not always match the thickness of the irradiated layer. Depending on the excitation wavelength (below the band gap, $\lambda$>150 nm), a part of the pristine layer may be excited as well. Anyway, we have not observed any new PL band after the irradiation, which is expected to produce defects in the spinel structure; moreover the deep-ultraviolet PLE bands above 7.5 eV were lost. In overall, from spectroscopic point of view, a non-negligible number density of antisites may be produced in the ceramics after irradiation. For example, the experimental uncertainty of the inversion $\Delta i$=0.01 corresponds to the antisites number density ~$10^{20}$ $cm^{-3}$, which can strongly affect PL spectra of non-irradiated ceramics. Because of the observed difference in PL/PLE spectra of the ceramics before and after irradiation, it was assumed that the natures of as-grown and radiation-induced defects are different. Our results confirm that possible effect of the antisite creation may be an alternation of the energy relaxation channels leading to the exciton quenching. On the other hand, weak transitions at E' = 7.25 ± 0.25 eV in UV1 PLE spectrum (Fig 6) may be connected to a disorder in pristine spinels, which is conserved after the irradiation.

The comparison of PLE spectra shows their significant modifications related to the intensity changes of several poor-resolved superposed bands of the sub-band gap electronic transitions in Ta-doped ceramics (Fig 7). The most striking features concern a strong weakening of UV1 PLE at 7.8 eV and intensification of PLE between 6.0 and 7.5 eV common for all other PL emissions UV2, V1 and V2, except for UV1 one (the seeming presence of this PLE band in UV1 PL is explained by a contribution of the intense broad UV2 PL, as shows PLE spectrum at $\lambda_{PL}$=240 nm in Fig. 7). We notice that PLE bands of pristine ceramics (Fig. 6) are still visible in PLE of Ta-doped ceramics at low intensity, superposed by this new dominant PLE band, which apparently originates from the grain boundary region enriched with Ta. The modification of the force of electronic transitions by Ta may be the reason. The irradiation provokes similar consequences on the PLE spectra, as in pristine spinel ceramics: the high energy part above 7.5 eV vanishes and that between 7.5 and 6.0 eV weakens.

The irradiation with $He^+$ ions permits an additional bands selection, helpful for understanding of the energy transfer process. The ratio of PLE spectra of F and $F^+$ centres of samples before and after the ionized irradiation

are shown in Fig. 8. The ratio in Ta-free ceramics (Fig. 8a) is close to 1 below energies of the excitonic transitions hν < 7.0 eV, which indicates a negligible modification of the related intra-gap states. In contrast, the PL ratio in the Ta-doped ceramics is close to 1 in the energy range below $E^*$=5.75 eV (Fig. 8b) while it increased to 4 at 7.0 eV. Consequently, two contributions can be resolved in this PLE analysis: 5.75 eV ≤ E" < 7 eV and 5 eV ≤ E"' < 5.75 eV. We assign E"' to the direct absorption of F / $F^+$ centres and E" to a common intermediate excited state, which transferred energy to these centres. We notice that a careful comparison of the PLE lineshapes showed an extension of $F^+$ band to lower energies compared with F band, which is in agreement with the energy shift of the respective absorptions at 5.3 and 4.75 eV [26]. The E" transitions are most probably located at the grain boundaries, since the energy transfer to the emitting F and $F^+$ states is strongly affected by Ta (UV2 and V1 in Figs 6 and 7). Our results showed that F/$F^+$ PL spectra are similar after excitation in the spectral range of the excitonic transitions (7.8 eV) and direct complex excitation (E"), which indicates an effective energy transfer exciton → complex → F/$F^+$. Moreover, the stronger PL attenuation in the range of E" transitions (Fig. 8b) indicates that Ta weakens the structure facilitating damage produced by $He^+$ ions. Summing up the results of XRD, EDX and PL measurements, the hypothetic Ta complex may be assigned with the nucleated $Mg_4Ta_2O_9$ phase.

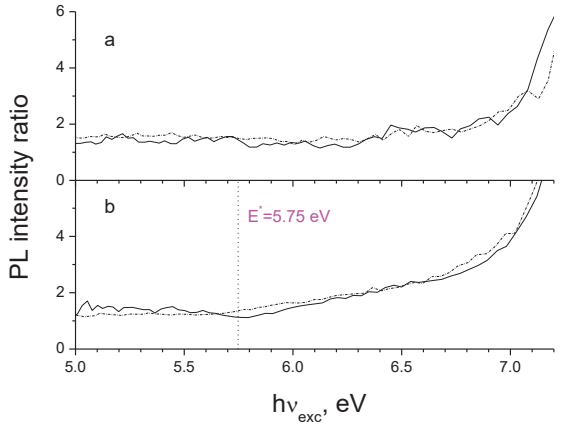


Fig. 8. Intensity ratio of PLE spectra before and after irradiation of $MgAl_2O_4$ ceramics without (a) and with 1 wt% $Ta_2O_5$ (b): UV2 band (F-centres, solid line) and V1 band ($F^+$-centres, dashed line) (T=9 K).

PL intensities of both F and $F^+$ centers were strongly intensified in Ta-doped ceramics (Fig 7) indicating, in agreement with the EDX analysis (Fig. 4), their preferential position at the grain boundaries. Consequently, antisites situated at the grain boundaries enriched with Ta can be proposed for the explanation of the E" band attenuation after $He^+$ irradiation. This alternation of the energy relaxation from interaction with bulk to interface states (after $He^+$ irradiation) may be a reason of the excitonic PL suppression. A stronger attenuation of the energy transfer from localized excitons E' (7.25 eV) can be also noticed, which according to Fig. 8 (a) and (b) was not appreciably sensitive to Ta doping. This band may therefore belong to exciton localized near bulk antisites.

An additional support to the conclusion about preferential position of F and $F^+$ centres at the grain boundaries in the sintered ceramics comes from the fact that the related PLE spectra are extremely weak in $MgAl_2O_4$ single crystals [27]. Their PL intensities with excitation below the band gap are almost conserved after the irradiation with $He^+$ ions indicating a small structural damage, since $F^+$ center is expected to readily interact with defects derived from the cation disorder in the spinel structure, forming clusters of various defect centers [15] affecting PL bands.

The UV1 band intensity is also significantly lower in our small grain ceramics compared to $MgAl_2O_4$ single crystals [25]. Its intensity is lower in Ta-doped ceramics as well (Fig. 5) with no change of the lineshape. Moreover, our observations showed that the excitonic PL suppression after $He^+$ irradiation is stronger in the ceramics than in single spinel crystals. This supports our conclusion about exciton quenching at the grain boundaries due to interactions with the Ta-spinel complex and radiation-induced antisites.

## 6. Conclusion

Photoluminescence (PL) properties of pristine $MgAl_2O_4$ spinel ceramics and those doped with $Ta_2O_5$ were investigated. The ceramics were prepared via spark plasma sintering method from commercial spinel powders and possessed an averaged degree of inversion i≈0.15. The irradiation of the prepared ceramics with $He^+$ ions of total dose $10^{17}$ $cm^{-2}$ was applied to check it consequence on the material damage. The PL spectra include five principal bands assigned to localized excitons (5.44 eV), F centers (3.9 eV), $F^+$ centers (3.0 eV), $Mn^{2+}$ (2.4 eV) and $Cr^{3+}$ (1.8 eV) impurities.

The results indicate strong influence of the grain boundaries on PL and PLE spectra. The Ta-doping promoted the appearance of O and Al vacancies at the grain boundaries leading to the formation of a large number density of $F^+$ centres, which provokes an inhibition of the excitonic PL and enhancement of that of F and $F^+$ centres. This is explained by an intermediate state (with electronic transitions in the spectral range between 5.75 eV and 7.0 eV) situated at the grain boundaries and structurally linked to Ta atoms, which was tentatively assigned to the nucleated $Mg_4Ta_2O_9$ phase; it interacts with excitons and effectively transfers energy to F and $F^+$ centres. The disorder of the spinel structure induced by $He^+$ ions irradiation results in the suppression of the excitonic PL and exciton energy transfer. This effect was attributed to an interaction of excitons with radiation-induced antisites situated at the grain boundaries. Consequently, the irradiation-induced displacements, effectively recombining in bulk spinel crystals [25], accumulate at the grain boundaries of the spinel ceramics. A weak residual PL

excitation band at 7.25±0.25 eV may belong to excitons localised near bulk antisites.

## Acknowledgments

This work has been carried out within the framework of the EUROfusion Consortium and French Research Federation for Fusion Studies and has received funding from the Euratom research and training programme 2014–2018 under grant agreement No. 633053. The views and opinions expressed herein do not necessarily reflect those of the European Commission. The authors are grateful to the SPS Platform Ile-de-France (France) and would like to thank B. Villeroy (ICMPE-CNRS, France) for his technical expertise and K. Mizohata for the irradiation of samples. Support from Estonian Research Council grant PUT PRG 619 is gratefully acknowledged.

## References

[1] K. E. Sickafus, L. Minervini, R. W. Grimes, J. A. Valdez, M. Ishimaru, F. Li, K. J. McClellan, T. Hartmann, Radiation tolerance of complex oxides, Science 289 (2000) 748-751.

[2] G. Ackland, Controlling Radiation Damage, Science 327 (2010) 1587-1588.

[3] X.-M. Bai, A. F. Voter, R. G. Hoagland, M. Nastasi, B. P. Uberuaga, Efficient Annealing of Radiation Damage Near Grain Boundaries via Interstitial Emission, Science 327 (2010) 1631-1634.

[4] K. K. Ohtaki, M. K. Patel, M. L. Crespillo, K. K. Karandikar, Y. Zhang, O. A. Graeve, M. L. Mecartney, Improved high temperature radiation damage tolerance in a three-phase ceramic with heterointerfaces, Sci. Rep. 8 (2018) 13993.

[5] Marcia R. Gallas, Bernard Hockey, Alexander Pechenik, Gasper J. Piermarini, Fabrication of Transparent γ- $Al_2O_3$ from Nanosize Particles, J. Am. Ser. Soc. 77 (1994) 2107-2112.

[6] J. A. Wollmershauser, B. N. Feigelson, E. P. Gorzkowski, C. T. Ellis, R. Goswami, S. B. Qadri, J. G. Tischler, F. J. Kub, R. K. Everett, An extended hardness limit in bulk nanoceramics, Acta Materialia 69 (2014) 9-16.

[7] M. M. Hasan, P. P. Dholabhai, S. Dey, B. P. Uberuaga, R. H. R. Castro, Reduced grain boundary energies in rare-earth doped $MgAl_2O_4$ spinel and consequent grain growth inhibition, J. Eur. Cer. Soc., 37 (2017) 4043-4050.

[8] A. Pille, M. Amamra, A. Kanaev, T. Billeton, E. Feldbach, F. Schoenstein, Morphology and luminescence of $MgAl_2O_4$ ceramics obtained via spark plasma sintering, Ceram. Int. 45 (2019) 8305-8312.

[9] J.-M. Kim, H.-N. Kim, Y.-J. Park, J.-W. Ko, J.-W. Lee, H.-D. Kim, Fabrication of transparent $MgAl_2O_4$ spinel through homogenous green compaction by microfluidization and slip casting, Ceram. Int. 41 (2015) 13354-13360.

[10] M. Kitaura, S. Tanaka, M. Itoh, A. Ohnishi, H. Kominami, K. Hara, Excitation process of $Ce^{3+}$ and $Eu^{2+}$ ions doped in $SrGa_2S_4$ crystals under the condition of multiplication of electronic excitations, J. Luminescence 172 (2016) 243-248.

[11] E. D. Bourret, D. M. Smiadak, R. B. Borade, Y. Ma, G. Bizarri, M. J. Weber, S. E. Derenzo, Scintillation of tantalate compounds, J. Lumin. 202 (2018) 332-338.

[12] Y. Baskin, D. C. Schell, Phase studies in the binary system MgO-$Ta_2O_5$, J. Am. Ceram. Soc. 46 (1963) 174-177.

[13] J. A Ball, M. Pirzada, R. W. Grimes, M. O. Zacate, D. W. Price, B. P. Uberuaga, J. Phys.: Condens. Matter 17 (2005) 7621-7631.

[14] V. T. Gritsyna, I. V. Afanasyev-Charkin, V. A. Kobyakov, Structure and electronic states of defects in spinel of different compositions $MgO{\cdot}nAl_2O_3$:Me, J. Am. Ceram. Soc. 82 (1999) 3365-3373.

[15] S. Sawai, T. Uchino, Visible photoluminescence from $MgAl_2O_4$ spinel with cation disorder and oxygen vacancy, J. Appl. Phys. 112 (2012) 103523.

[16] O. A. Plaksin and V. A. Stepanov, Radiation-induced electrical and optical processes in materials based on $Al_2O_3$, Opt. Spectrosc. 90 (2001) 542-551.

[17] W.-J. Chun, A. Ishikawa, H. Fujisawa, Tsuyoshi Takata, Junko N. Kondo, M. Hara, M. Kawai, Y. Matsumoto, K. Domen, Conduction and valence band positions of $Ta_2O_5$, TaON, and $Ta_3N_5$ by UPS and electrochemical methods, J. Phys. Chem. B 107 (2003) 1798-1803.

[18] M. L. Bortz, R. H. French, D. J. Jones, R. V. Kasowski, F. S. Ohuchi, Temperature dependence of the electronic structure of oxides: MgO, $MgAl_2O_4$ and $Al_2O_3$, Phys. Scr. 41 (1990) 537-541.

[19] M. E. Thomas, W. J. Tropf, S. L. Gilbert, Vacuum-ultraviolet characterization of sapphire, ALON, and spinel near the band gap", Opt. Eng. 32 (1993) 1340-1343.

[20] S. M. Hosseini, Structural, electronic and optical properties of spinel $MgAl_2O_4$ oxide, Phys. Stat. Sol. B 245 (2008) 2800-2807.

[21] G. Prieditis, E. Feldbach, I. Kudryavtseva, A. I. Popov, E. Shablonin and A. Lushchik, Luminescence characteristics of magnesium aluminate spinel crystals of different stoichiometry, IOP Conf. Ser.: Mater. Sci. Eng. 503 (2019) 012021.

[22] E. Feldbach, I. Kudryavtseva, K. Mizohata, G. Prieditis, J. Räisänen, E. Shablonin, A. Lushchik, Optical characteristics of virgin and proton-irradiated ceramics of magnesium aluminate spinel, Opt. Mat. 96 (2019) 109308.

[23] N. Mironova-Ulmane, V. Skvortsova, A. Pavlenko, E. Feldbach, A. Lushchik, Ch. Lushchik, V. Churmanov, D. Ivanov, V. Ivanov, E. Aleksanyan, Luminescence and EPR spectroscopy of neutron-irradiated single crystals of magnesium aluminium spinel, Rad. Measurements 90 (2016) 122-126.

[24] E. Feldbach, E. Toldsepp, M. Kirm, A. Lushchik, K. Mizohata, J. Räisänen, "Radiation resistance diagnostics of wide-gap optical materials", Opt. Mater. 55 (2016) 164-167.

[25] K. E. Sickafus, A. C. Larson, N. Yu, M. Nastasi, G. W. Hollenberg, F. A. Garner, R. C. Bradt, Cation disorder in high dose, neutron-irradiated spinel, J. Nucl. Mater. 219 (1995) 128-134.

[26] G. P. Summers, G. S. White, K. H. Lee, J. H. Crawford, Radiation damage in $MgAl_2O_4$, Phys. Rev. B 21 (1980) 2578-2584.

[27] L. Museur, E. Feldbach, M. Kitaura, A. Kanaev, UV-visible spectroscopy of $MgAl_2O_4$ spinel single crystal, UVSOR Annual report 2018, Nagoya, Japan.

↑ If possible equalize columns on the last page ↑

Tables

Table 1. Mass density of spinel ceramics with different $Ta_2O_5$ addition.

| d (wt%) | 0 | 0.5 | 1 | 2 | 4 |
|---|---|---|---|---|---|
| $\rho$ ($g.cm^{-3}$) | 3.575(6) | 3.540(7) | 3.563(8) | 3.586(9) | 3.594(5) |
| $\rho/\rho_0$ (%) | 99.9(2) | 99.0(2) | 99.6(2) | 100.2(2) | 100.4(1) |

Figure captions

Fig. 1. Sintering cycle applied to $MgAl_2O_4$ ceramics preparation. Times of P-T application are indicated below cycle lines.

Fig. 2. X-ray diffraction patterns of $MgAl_2O_4$ ceramics (Ta doping is indicated). Peaks of $MgAl_2O_4$ (●), $Mg_4Ta_2O_9$ (■) and MgO (x) phases are labelled. Inset shows $Mg_4Ta_2O_9$ peaks already at 1 wt% $Ta_2O_5$ doping.

Fig. 3. SEM images of $MgAl_2O_4$ ceramics with 0.5 wt% (a) and 1 wt% $Ta_2O_5$.

Fig. 4. SEM and EDX elemental maps of $MgAl_2O_4$ ceramics with 1 wt% $Ta_2O_5$. A representative zone of Ta enrichment and lack of O and Al elements is shown by dotted circle.

Fig. 5. PL spectra of non-irradiated $MgAl_2O_4$ ceramics without (a) and with 1 wt% $Ta_2O_5$ (b) addition (excitation at 157 nm, T=9 K).

Fig. 6. PLE spectra of pure $MgAl_2O_4$ ceramics before (blue) and after (magenta) $He^+$ irradiation. PL bands and respective wavelengths are indicated (T=9 K).

Fig. 7. PLE spectra of $MgAl_2O_4$ ceramics with 1 wt% $Ta_2O_5$ before (blue, gray) and after (magenta) $He^+$ irradiation. PL bands and respective wavelengths are indicated (T=9 K).

Fig. 8. Intensity ratio of PLE spectra before and after irradiation of $MgAl_2O_4$ ceramics without (a) and with 1 wt% $Ta_2O_5$ (b): UV2 band (F-centres, solid line) and V1 band ($F^+$-centres, dashed line) (T=9 K).